Journal of Structural Engineering Vol.45A(March 1999) JSCE

Complex-Mode Buffeting Analysis of Long-Span Bridges II Extensive Formulation and Further Results

Nguyen Nguyen Minh*, Hitoshi Yamada** and Toshio Miyata***

* Former Graduate Student, Dept. of Civil Eng., Yokohama National University
** Professor, Dept. of Civil Engineering, Yokohama National University
*** Professor, Dept. of Civil Engineering, Yokohama National University

This paper is the extension of a paper in the last issue of this journal, in which the state of the art of an analytical approach for buffeting response of long-span bridges by complex modes has been presented. In this paper, the method, which is herein named Aeroelastic Complex Mode method will be extensively developed in details. The calculation scheme is based on the direct complex eigen-analysis of the integrated system between the three-dimensional FEM model of a long-span bridge and the aeroelastic effects. Actual vibrational modes of the bridge in wind flow, which are called Aeroelastic Complex Modes, thus can be appropriately determined at each mean wind speed. A Complex Modal Analysis scheme is then formulated for buffeting analysis in both time and frequency domains. Coupled buffeting responses of the Akashi-Kaikyo Bridge model is then effectively analyzed by the present method. Further results, parameter studies and comparison with the conventional buffeting method are provided.

Key Words: coupled buffeting, complex eigen-analysis, complex mode, aeroelastic effect

1. Introduction

The Akashi Kaikyo Bridge, now the longest suspension bridge in the world with the main span of 1991m, has been successfully realized. In the design of the bridge, a full model test in a large boundary layer wind tunnel has been conducted, from which many interesting findings on the dynamic behaviors of the bridge were experimentally obtained[11]. Under the action of turbulent flows, the full model of the bridge exhibited a strongly coupled three-dimensional vibration with remarkable signs of aeroelastic phenomenon. Prediction of such buffeting responses therefore emerges as a major consideration in the design of all long-span bridges.

In the past, a couple of methods for predicting coupled buffeting response of long-span bridges has been proposed. However, these methods, mostly following the modal analysis technique, have performed the analysis using the set of *mechanical modes*, which mean the modes of the bridge system determined at no wind condition. It is obvious that due to the aeroelastic effects, the mechanical modes are not the actual vibration modes of the bridge vibrating in wind flows. Such analyses are therefore rendered much complicated by mathematical formulations or transformation techniques to incorporate the aeroelastic effects.

In this regard, the Direct FEM Flutter Analysis Method by Miyata and Yamada[9] (1988), and one of its developments - the Mode Tracing Method by Dung et al.[2] (1996) for flutter prediction could provide a better representation of the dynamic behaviors of long span bridges in term of *complex modes*. Complex eigen-analysis is directly made for an integrated system consisting of the 3-D FEM model of a full bridge and the aeroelastic effects caused by the wind flow, resulting in the complex modes, which are apparently the actual vibrational modes of the bridge in wind flow. The effectiveness and importance of the complex modes in predicting the flutter wind speed and flutter mode shape of long span bridges have been well confirmed and reported (Miyata et al.[10] 1995, Dung et al.[3] 1997).

In this study, an approach for buffeting analysis of long-span bridges using the complex modes is developed. The state of the art of the approach has been presented in a paper in this journal last year (Minh et al.[7] 1998). However, there remained a couple of points in the formulation, which needs to be clarified and proved. In this paper, the method will be extensively presented in details to provide a step-by step formulation for ease of following and programming. The complex modes are herein re-named *aeroelastic complex modes* to indicate the fact that the aeroelastic effects are inherently incorporated. By employing the Mode Tracing Method[2], the aeroelastic complex modes at a certain wind speed can be obtained. The modal decomposition then can be made straightforward by a complex modal analysis scheme. A comparative consideration in the frequency-domain formulation is considered in terms of the cross-terms of the modal-force spectral matrix, and then their effects on the buffeting response are investigated.

Further new results on the coupled buffeting of the Akashi Kaikyo Bridge model with refined input data are presented and interpreted. A check on the effects of the Von-Karman coherence on the response, and comparison with the conventional buffeting method by Davenport[1] (1962) are extensively carried out.

2. Complex Modal Analysis

2.1. *Complex Eigen-Analysis*

The Direct FEM Flutter Analysis[9] formulation and the Mode Tracing Method[2] are employed for complex eigen-analysis. The equation of motion of a full-model bridge in the presence of aeroelastic phenomena can be expressed as,

$$\mathbf{M}\ddot{\mathbf{u}} + \mathbf{C}\dot{\mathbf{u}} + \mathbf{K}\mathbf{u} = \mathbf{F}_{ae} + \mathbf{F}_b \tag{1}$$

where **M**, **K** are mass and stiffness matrices formed by Finite Element method, **u** is displacement vector, $\mathbf{F}_{ae}$ is the motion-dependent self-excited force depending on reduced frequency K=ωB/U (ω is circular frequency and U is mean wind speed), and $\mathbf{F}_b$ is the buffeting force. Other notations are depicted in Fig.1.

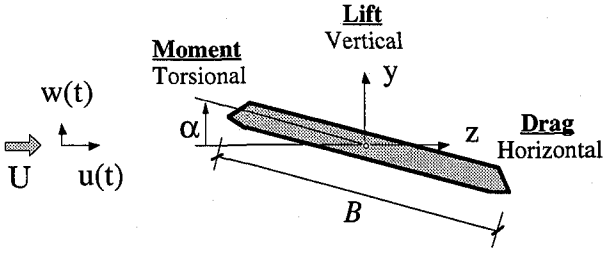

Fig.1 Sectional model of bridge deck

Assume harmonic oscillation, $\mathbf{f}_{ae}$, which is the self-excited force for a section of bridge deck with unit length in local coordinates, can be expressed following Direct FEM Flutter Analysis[9] formulation as follows,

$$\mathbf{f}_{ae} = \begin{Bmatrix} L_{ae} \\ D_{ae} \\ M_{ae}/B \end{Bmatrix} = \mathbf{F}_w \begin{Bmatrix} \ddot{y} \\ \ddot{z} \\ \ddot{\alpha}B \end{Bmatrix} = \mathbf{F}_w \ddot{\mathbf{w}} \tag{2}$$

where **w** is displacement vector in local coordinate, in which y, z, and α is vertical, horizontal displacement and rotational angle as depicted in Fig.1; and

$$\mathbf{F}_w = -(\rho\pi B^2)\begin{bmatrix} L_{yR}+iL_{yI} & L_{zR}+iL_{zI} & L_{\alpha R}+iL_{\alpha I} \\ D_{yR}+iD_{yI} & D_{zR}+iD_{zI} & D_{\alpha R}+iD_{\alpha I} \\ M_{yR}+iM_{yI} & M_{zR}+iM_{zI} & M_{\alpha R}+iM_{\alpha I} \end{bmatrix} \tag{3}$$

in which L_{ae}, D_{ae}, M_{ae} are aeroelastic lift, drag and moment respectively; ρ is air density; $\mathbf{F}_w$ contains a full set of 9-complex unsteady coefficients[9),10)] (or equivalently[4),8)] 18 flutter derivatives[5)]), which exclusively depend on reduced frequency K. The local $\mathbf{f}_{ae}$ distributing along the bridge deck can be lumped for each section to concentrate to each shear node. The local nodal forces, which is expressed in Appendix A, then can be transformed into the global coordinate through FEM scheme, and assembled to form the global self-excited vector $\mathbf{F}_{ae}$, which can be expressed by,

$$\mathbf{F}_{ae} = \sum^{n} \kappa(\mathbf{F}_w \ddot{\mathbf{w}}) = \mathbf{F}_w^G \ddot{\mathbf{u}} \tag{4}$$

where the operator κ(.) indicates the transforming process from local to global coordinate and the sigma sign expresses the assembly process in FEM scheme for n elements. As the results, $\mathbf{F}_{ae}$ is function of the global acceleration vector $\ddot{\mathbf{u}}$ so that it can be integrated into the left-hand side as an additional complex mass. Neglecting the damping matrix **C**, Eq.(1) can be rewritten as

$$(\mathbf{M} - \mathbf{F}_w^G)\ddot{\mathbf{u}} + \mathbf{K}\mathbf{u} = \mathbf{F}_b \tag{5a}$$

or,

$$\mathbf{M}_F\ddot{\mathbf{u}} + \mathbf{K}\mathbf{u} = \mathbf{F}_b \tag{5b}$$

The term $\mathbf{F}_b$ can be dropped for the eigen-analysis of the system. Assume harmonic response for the free vibration of **u** with complex frequency λ,

$$\mathbf{u} = \mathbf{A}e^{i\lambda t} \tag{6a}$$

from which,

$$\ddot{\mathbf{u}} = -\lambda^2\mathbf{A}e^{i\lambda t} \tag{6b}$$

Then the equation of complex eigen-problem is formed,

$$\det\left|\mathbf{K} - \mathbf{M}_F(K)\times\lambda^2\right| = 0 \tag{7a}$$

where

$$K = \frac{\omega B}{U} \tag{7b}$$

in which the modal frequency ω is the module of $\sqrt{\lambda^2}$ (square-root of the complex eigenvalue). In $\mathbf{M}_F$, the self-excited force is integrated. Therefore $\mathbf{M}_F$ is a complex function of the reduced frequency K, which depends on wind speed U and the unknown modal frequencies ω.

To solve the complex eigen-problem in Eq.(7) to obtain a set of aeroelastic complex modes at a certain wind speed U, the Mode Tracing Method is employed. Details of the method can be found from Dung et al.[2] (1996). However, for ease of programming, the procedure of the method is recast and introduced in Appendix B. The method considers only *one mode* at a time and then traces the evolution of the modal properties with step-by-step increase of wind speed. The modal properties of every mode are therefore determined *at the same wind speeds, which can be specified by the analyst.* A simple application of this method for a set of aeroelastic modes at a desired wind speed U is to trace mode by mode from U=0 to the desired wind speed to collect the result; and such a procedure can be repeated for all interested wind speeds. However, if the number of interested wind speeds is decided, the procedure to obtain their sets of aeroelastic complex modes can be made much faster by only one-time tracing mode by mode from U=0 to the maximum interested wind speed. The wind speed steps are chosen coinciding with the interested wind speeds so that their aeroelastic modal properties can be evaluated and collected in the process of the method. An example can be seen from Fig.4. The modal aerodynamic damping and modal frequency are traced successively at 20 specified wind speeds, ranging from 5 to 100 m/s, including eight interested wind speeds of 30, 36, 44, 54, 63, 71, 76 and 80 m/s. The sets of aeroelastic complex modes at the eight interested wind speeds thus can be obtained by appropriately collecting during the calculation process, and storing in the memory for later use.

2.2. *Uncouple Equation of Motion*

The modal decomposition for Eq.(5b) at a certain wind speed then can be performed by using corresponding eigenvectors. Since $\mathbf{M}_F$ is complex and not symmetric, two *biorthogonal* sets of complex eigenvectors, left $\mathbf{v}_L$ and right $\mathbf{v}_R$, exist for the modal decomposition. Note that the results from the Mode Tracing Method are only the complex eigenvalue λ_n^2 and the right eigenvector $\mathbf{v}_{Rn}$, which are resulted from,

$$\mathbf{K}\mathbf{v}_{Rn} = \lambda_n^2 \mathbf{M}_F \mathbf{v}_{Rn} \tag{8}$$

This equation is equivalent to Eq.(7a). The left eigenvector will be the solution from,

$$\mathbf{K}\mathbf{v}_{Lm} = \lambda_m^2 \mathbf{M}_F^T \mathbf{v}_{Lm} \tag{9}$$

Note that since the determinant of a matrix is equal to that of its transpose, it follows that a matrix has the same eigenvalue as its transpose. Then the eigenvalues in both Eqs.(8) and (9) for a mode are the same. The left eigenvector therefore can be easily obtained along the process of the Mode Tracing method as long as the corresponding eigenvalue is available. It is worthy to note that the left and the right eigenvectors will be identical at U=0, at which the matrix $\mathbf{M}_F$ is symmetric, to become the mechanical mode shape. As wind speed increases, these two eigenvectors will gradually change into quite different shapes to each other, as typically seen on Fig.2. Transpose of Eq.(9), making use of the symmetry of $\mathbf{K}$, yields,

$$\mathbf{v}_{Lm}^T \mathbf{K} = \lambda_m^2 \mathbf{v}_{Lm}^T \mathbf{M}_F \tag{10}$$

Post-multiply both sides of Eq.(10) with a right eigenvector, and pre-multiply both sides of Eq.(8) with the transpose of a left eigenvector give,

$$\begin{aligned} \mathbf{v}_{Lm}^T \mathbf{K} \mathbf{v}_{Rn} &= \lambda_m^2 \mathbf{v}_{Lm}^T \mathbf{M}_F \mathbf{v}_{Rn} \\ \mathbf{v}_{Lm}^T \mathbf{K} \mathbf{v}_{Rn} &= \lambda_n^2 \mathbf{v}_{Lm}^T \mathbf{M}_F \mathbf{v}_{Rn} \end{aligned} \tag{11}$$

from which the *bi-orthogonality* of the left and right eigenvectors with respect to $\mathbf{M}_F$ and $\mathbf{K}$ is proved,

$$\begin{aligned} \mathbf{v}_{Lm}^T \mathbf{K}\ \mathbf{v}_{Rn} &= 0 \\ \mathbf{v}_{Lm}^T \mathbf{M}_F \mathbf{v}_{Rn} &= 0 \end{aligned} \qquad \text{if } m \neq n \tag{12}$$

To facilitate the modal decomposition, the left and the right eigenvectors are normalized in such a way that,

$$\mathbf{v}_{Lm}^T \mathbf{v}_{Rm} = 1 \tag{13}$$

The modal decomposition for Eq.(5b) now can be made. The uncoupled equation of motion in generalized coordinate $\mathbf{r}$ can be written as,

$$(\mathbf{v}_L^T \mathbf{M}_F \mathbf{v}_R)\ddot{\mathbf{r}} + (\mathbf{v}_L^T \mathbf{K}\ \mathbf{v}_R)\mathbf{r} = \mathbf{v}_L^T \mathbf{F}_b \tag{14}$$

where

$$\mathbf{u} = \mathbf{v}_R\, \mathbf{r} \tag{15}$$

By Eq.(12), the uncouple equation Eq.(14) can be written as,

$$\ddot{r}_n + \lambda_n^2 r_n = \frac{f_{bn}}{m_n} \tag{16}$$

where,

modal mass $\quad m_n = \mathbf{v}_{Ln}^T \mathbf{M}_F \mathbf{v}_{Rn}$ (17a)

modal stiffness $\quad k_n = m_n \lambda_n^2 = \mathbf{v}_{Ln}^T \mathbf{K}\ \mathbf{v}_{Rn}$ (17b)

modal force $\quad f_{bn} = \mathbf{v}_{Ln}^T \mathbf{F}_b$ (17c)

The relation between modal stiffness with modal mass and eigenvalue in Equation (17b) is resulted from Eq.(11). From Eq.(14), it can be seen that the left eigenvectors decide the contribution of external forces to each mode, whereas the right eigenvectors express the mode shapes. By their biorthogonality, the equation of motion can be uncoupled as in Eq.(16). However, the stiffness or frequency in this equation is still complex. The square of complex frequency (or eigenvalue) λ_n^2 implied the existence of a frequency phase lag representing for the *aerodynamic damping* in the vibration, which makes the Eq.(16) difficult to be solved by a common technique of dynamic analysis. Therefore, further derivations should be made to extract the modal damping and modal frequency explicitly in *real* values.

Write the complex frequency (square root of the complex eigenvalue) into its real and imaginary parts, $\lambda_n = \lambda_{Rn} + i\,\lambda_{In}$, where $i = \sqrt{-1}$, and consider the second term of the left hand side of Eq.(16),

$$\begin{aligned} \lambda_n^2 r_n &= (\lambda_{Rn} + i\lambda_{In})^2 r_n \\ &= \left[(\lambda_{Rn}^2 + \lambda_{In}^2) + 2\lambda_{In} i(\lambda_{Rn} + i\lambda_{In})\right] r_n \end{aligned} \tag{18}$$

From the harmonic motion assumption in Eq.(6a) and the transforming Eq.(15), the following relation holds,

$$\dot{r}_n = i\lambda_n r_n = i(\lambda_{Rn} + i\lambda_{In}) r_n \tag{19}$$

Substitute Eq.(19) into Eq.(18),

$$\lambda_n^2 r_n = (\lambda_{Rn}^2 + \lambda_{In}^2) r_n + 2\lambda_{In} \dot{r}_n \tag{20}$$

By this new expression of the second term, Eq.(16) can be rearranged in a more convenient and explicit form as,

$$\ddot{r}_n + 2\xi_{aen}\omega_n \dot{r}_n + \omega_n^2 r_n = Q_{bn} \tag{21}$$

where normalized buffeting force $Q_{bn}=f_{bn} / m_n$. The modal aerodynamic damping ratio ξ_{aen} and modal frequency ω_n here are *real* values as follows,

$$\omega_n = \sqrt{\lambda_{Rn}^2 + \lambda_{In}^2}\ ; \quad \xi_{aen} = \lambda_{In} / \sqrt{\lambda_{Rn}^2 + \lambda_{In}^2} \tag{22}$$

At this stage, under the assumption of proportional damping, the structural damping can be incorporated in the form of *modal structural damping ratio* ξ_{sn}. The final form of the uncouple equation of motion then is

$$\ddot{r}_n + 2(\xi_{aen} + \xi_{sn})\omega_n \dot{r}_n + \omega_n^2 r_n = Q_{bn} \tag{23}$$

or,

$$\ddot{r}_n + 2\xi_n \omega_n \dot{r}_n + \omega_n^2 r_n = Q_{bn} \tag{24}$$

in which ξ_n is the total modal damping ratio. In Eq.(24), the general coordinate r_n together with its derivatives and the normalized modal force Q_{bn} are complex, but the modal damping and modal frequency are already expressed explicitly in real values, which makes it easy to solve the equation. The most important advantage of this

equation of motion (24) when compared to those of other existing method[4),5)] is that it is *completely uncoupled* at a mean wind speed, so that it can be flexibly solved in either time or frequency domain. This advantage is thanks to the use of the aeroelastic complex modes, in which the aeroelastic effects have been incorporated.

3. Time Domain Analysis

The wind field can be modeled as comprising of a mean wind speed and turbulent components as seen in Fig.1. By the quasi-steady assumption[1),5)], the buffeting force $\mathbf{F}_b$ can be computed from horizontal (u) and vertical (w) turbulent velocity components as follows

$$\mathbf{F}_b=\begin{Bmatrix} L_b \\ D_b \\ M_b/B \end{Bmatrix} = \frac{\rho U B}{2}\begin{bmatrix} 2C_L & (C_L'+C_D) \\ 2C_D & C_D' \\ 2C_M & C_M' \end{bmatrix}_{\alpha_0} \begin{Bmatrix} u(t) \\ w(t) \end{Bmatrix} \quad (25)$$

where L_b, D_b, M_b are buffeting lift, drag and moment, respectively. C_L, C_D, C_M are static coefficients for lift, drag and moment, respectively. The prime (') denotes their derivatives with respect to the angle of attack of the mean wind speed on the section model (Fig.1). Values of these coefficients at the mean angle of attack α_0 are used. The context of the approach thus involves the work of numerical simulation of turbulence u(t) and w(t). Details of this work can be found in Minh et al.[6)] (1997).

The buffeting analysis is then carried out by Newmark direct integration method for Eq.(24). The time history of the generalized displacement **r** in modal space is obtained, and then can be transformed by Eq.(15) into the time-histories of physical displacement responses, including vertical, horizontal and torsional components at any node along the bridge deck. The RMS and ensemble average of maximum amplitude of the responses then can be evaluated directly from the response time-histories.

It is noted that for N modes, Eq.(24) is equivalent to N complex equations. Each complex equation can be considered as including 2 separate equations, one real and one imaginary. The direct integration therefore, in principle, should be made for totally 2N equations. However, for the uncouple equation of motion Eq.(24), all operations in the direct integration are linear for coordinate **r** and the normalized buffeting force, so that the integration can be made directly on the N complex equations with complex variables.

4. Frequency Domain Analysis

Denote the Fourier Transform, e.g. for the generalized coordinate r by,

$$\bar{r}_n = \int_0^\infty r_n e^{-i\omega t} dt \quad (26)$$

Then the equation of motion in frequency domain can be expressed as,

$$\left(-\omega^2 + 2\xi_n\omega_n\omega + \omega_n^2\right)\bar{r}_n = \frac{1}{m_n}\bar{f}_{bn} \quad (27)$$

or in matrix form,

$$\mathbf{E}\bar{\mathbf{r}} = \bar{\mathbf{Q}}_b \quad (28)$$

Apparently, the impedance matrix **E** here is completely diagonal. The general term is

$$E_{nn} = -\omega^2 + i\left(2\xi_n\omega_n\right)\omega + \omega_n^2 \quad (29)$$

In general, there are two ways to solve the set of uncouple equations of motion in frequency domain: Multi-degree-of-freedom (MDOF) spectral formulation or Single-degree-of-freedom (SDOF) spectral formulation.

4.1. MDOF Spectral Formulation

The MDOF spectral formulation develops the whole set of equations of motion simultaneously by its matrix form of Eq.(28) into the spectral form using standard random vibration analysis for MDOF system. The hermitian transpose of Eq.(28) is,

$$\bar{\mathbf{r}}^H\mathbf{E}^H = \bar{\mathbf{Q}}_b^H \quad (30)$$

post-multiplying Eq.(30) to Eq.(28) yields,

$$\mathbf{E}\,\bar{\mathbf{r}}\,\bar{\mathbf{r}}^H\mathbf{E}^H = \bar{\mathbf{Q}}_b\bar{\mathbf{Q}}_b^H \quad (31)$$

from which the PSD matrix for the generalized coordinate **r** can be developed and expressed by,

$$\mathbf{S}_{rr}(\omega) = \mathbf{E}^{-1}\mathbf{S}_{Q_bQ_b}\left[\mathbf{E}^H\right]^{-1} \quad (32)$$

where $\mathbf{S}_{QbQb}$ is the power spectral density (PSD) matrix for modal buffeting force. The generalized response **r** can be obtained in term of its PSD matrix $\mathbf{S}_{rr}(\omega)$ by solving Eq.(32), as long as the PSD matrix of the modal buffeting force is available. There existed a developed form of the PSD of modal buffeting force by mechanical modes in real number for bridge analysis in Jain et al.[5)] (1996). However, since the aeroelastic modes here are complex and separated into left and right eigenvectors, necessary derivations consistent with complex modal analysis must be made.

Let $y_{Ln}(x)$, $z_{Ln}(x)$ and $\alpha_{Ln}(x)$ are respectively the vertical, horizontal and torsional components of the complex *left eigenvector* of n^{th} mode at span location x. The complex modal buffeting force can be expressed as,

$$f_{bn}(t) = \int_0^L \left[L_b(t)y_{Ln} + D_b(t)z_{Ln} + \frac{M_b(t)}{B}\alpha_{Ln}\right]dx \quad (33)$$

then its Fourier Transform into frequency ω domain at span location x_A is,

$$\bar{f}_{bn}(x_A,\omega) = \int_0^L \left[\bar{L}_b(\omega)y_{Ln}(x_A) + \bar{D}_b(\omega)z_{Ln}(x_A) + \frac{\bar{M}_b(\omega)}{B}\alpha_{Ln}(x_A)\right]dx \quad (34)$$

Make Fourier Transform for Eq.(25), then substitute the Fourier transform of buffeting force into Eq.(34), one obtains,

$$\bar{f}_{bn}(x_A,\omega) = \frac{1}{2}\rho U B\int_0^L \Omega(x_A,\omega)dx \quad (35)$$

where

$$\Omega = 2\left[C_L y_{Ln}(x_A) + C_D z_{Ln}(x_A) + C_M\alpha_{Ln}(x_A)\right]\bar{u}(\omega) + \left[(C_D' + C_L)y_{Ln}(x_A) + C_D' z_{Ln}(x_A) + C_M'\alpha_{Ln}(x_A)\right]\bar{w}(\omega)$$

The following matrix equation then can be obtained for N complex modes, where n and m are index of modes,

$$\overline{Q}_{bn}\overline{Q}_{bm}^{H}=\left(\frac{1}{2}\rho UB\right)^{2}\times\frac{1}{m_n m_m^{*}}\int_0^L\int_0^L \bar{f}_{bn}\bar{f}_{bm}^{*}dx_A dx_B \tag{36}$$

from which the power spectral density (PSD) matrix can be developed. The asterisk denotes the complex-conjugate operation. The general term of the PSD matrix of the modal buffeting force then can be written as,

$$S_{Q_{bn}Q_{bm}^{H}}(\omega)=\left(\frac{\rho UB}{2}\right)^{2}\frac{1}{m_n m_m^{*}}\int_0^L\int_0^L \Psi(x_A,x_B,\omega)dx_A dx_B \tag{37}$$

where

$$\begin{aligned}\Psi(x_A,x_B,\omega)=&\left\{\tilde{q}_n(x_A)\tilde{q}_m^{*}(x_B)S_{uu}(x_A,x_B,\omega)\right.\\&+\tilde{s}_n(x_A)\tilde{s}_m^{*}(x_B)S_{ww}(x_A,x_B,\omega)\\&+\left[\tilde{q}_n(x_A)\tilde{s}_m^{*}(x_B)+\tilde{s}_n(x_A)\tilde{q}_m^{*}(x_B)\right]C_{uw}(x_A,x_B,\omega)\\&\left.+i\left[\tilde{q}_n(x_A)\tilde{s}_m^{*}(x_B)-\tilde{s}_n(x_A)\tilde{q}_m^{*}(x_B)\right]Q_{uw}(x_A,x_B,\omega)\right\}\end{aligned} \tag{38}$$

L is bridge's length; x_A, x_B are span locations; S_{uu}, S_{ww}, S_{uw} are respectively uu-cross-spectrum, ww-cross-spectrum and uw-cross-spectrum between 2 points x_A and x_B; $S_{uw}=C_{uw}+iQ_{uw}$; with C_{uw} being cospectrum and Q_{uw} being quadrature spectrum; and

$$\tilde{q}_n(x)=2\left[C_L y_{Ln}(x)+C_D z_{Ln}(x)+C_M\alpha_{Ln}(x)\right] \tag{39a}$$

$$\tilde{s}_m(x)=\left(C_L'+C_D\right)y_{Lm}(x)+C_D' z_{Lm}(x)+C_M'\alpha_{Lm}(x) \tag{39b}$$

With the PSD matrix of buffeting force by Eq.(37), the PSD matrix for generalized response $\mathbf{S}_{rr}$ can be solved by Eq.(32). To turn to physical response $\mathbf{u}$, develop Eq.(15) into spectral form,

$$\mathbf{S}_{uu}=\mathbf{v}_R\mathbf{S}_{rr}\mathbf{v}_R^{H} \tag{40}$$

Then, the PSD for physical displacements at span location x are

$$S_{yy}(x,\omega)=\sum_n\sum_m y_{Rn}(x)y_{Rm}^{*}(x)S_{nrm}(\omega) \tag{41a}$$

$$S_{zz}(x,\omega)=\sum_n\sum_m z_{Rn}(x)z_{Rm}^{*}(x)S_{nrm}(\omega) \tag{41b}$$

$$S_{\alpha\alpha}(x,\omega)=\sum_n\sum_m B^{-2}\alpha_{Rn}(x)\alpha_{Rm}^{*}(x)S_{nrm}(\omega) \tag{41c}$$

where $y_{Rn}(x)$, $z_{Rn}(x)$ and $\alpha_{Rn}(x)$ are respectively the vertical, horizontal and torsional components of the *right eigenvector* of the n^{th} mode at span location x.

The mean-square values of buffeting response then can be evaluated by taking the integration of the physical displacement PSD with respect to frequency $f=\omega/2\pi$,

$$\sigma_y^2(x_A,x_B)=\int_0^\infty S_{yy}(x_A,x_B,f)df \tag{42a}$$

$$\sigma_z^2(x_A,x_B)=\int_0^\infty S_{zz}(x_A,x_B,f)df \tag{42b}$$

$$\sigma_\alpha^2(x_A,x_B)=\int_0^\infty S_{\alpha\alpha}(x_A,x_B,f)df \tag{42c}$$

The covariance matrices for y, z and α are then obtained, from which only the variance terms, which are calculated by $x_A=x_B$, are necessary since they indicate the mean square of responses at different location along the bridge deck.

The expected values of the maximum vibrational response occurring in the time interval T is (Davenport[1] 1962),

$$p_{max}(x)=k_p(x)\sigma_p(x) \tag{43}$$

where p stands for y, z or α displacement component; σ_p is the root-mean-square of p-component response; k_p is the respective peak factor, which can be estimated as

$$k_p(x)=\left[2\ln\nu(x)T\right]^{1/2}+\frac{0.577}{\left[2\ln\nu(x)T\right]^{1/2}} \tag{44}$$

in which

$$\nu(x)=\left[\frac{\int_0^\infty f^2 S_{pp}(x,f)df}{\int_0^\infty S_{pp}(x,f)df}\right]^{1/2} \tag{45}$$

$S_{pp}(x,f)$ is calculated from Eqs (41a,b,c) with ω replaced by real frequency f. In the statistic sense, the expected maximum vibrational amplitude in Eq.(43) can be treated equivalent to the ensemble average maximum amplitude in the time domain analysis for comparison.

4.2. SDOF Spectral Formulation

The SDOF spectral formulation develops each modal equation (27) into spectral form separately following the standard random vibration analysis for an SDOF system, and then solves for the physical responses' spectra and RMS induced by the mode. The SDOF spectral formulation therefore can be deduced from the MDOF spectral formulation as a special case in which the cross-terms of PSD matrix of the modal buffeting force are neglected. The procedure for SDOF spectral formulation is then similar to the MDOF spectral formulation with following two revisions,

(a) The PSD matrix of modal buffeting force is diagonal, then Eqs. (37), (38) are revised as the general term for the diagonal elements as follows,

$$S_{Q_{bn}Q_{bn}^{H}}(\omega)=\left(\frac{\rho UB}{2}\right)^{2}\frac{1}{m_n m_n^{*}}\int_0^L\int_0^L \Psi(x_A,x_B,\omega)dx_A dx_B \tag{46}$$

where

$$\begin{aligned}\Psi(x_A,x_B,\omega)=&\left\{\tilde{q}_n(x_A)\tilde{q}_n^{*}(x_B)S_{uu}(x_A,x_B,\omega)\right.\\&+\tilde{s}_n(x_A)\tilde{s}_n^{*}(x_B)S_{ww}(x_A,x_B,\omega)\\&+\left[\tilde{q}_n(x_A)\tilde{s}_n^{*}(x_B)+\tilde{s}_n(x_A)\tilde{q}_n^{*}(x_B)\right]C_{uw}(x_A,x_B,\omega)\\&\left.+i\left[\tilde{q}_n(x_A)\tilde{s}_n^{*}(x_B)-\tilde{s}_n(x_A)\tilde{q}_n^{*}(x_B)\right]Q_{uw}(x_A,x_B,\omega)\right\}\end{aligned} \tag{47}$$

(b) The PSD for physical displacements at span location x are

$$S_{yy}(x,\omega)=\sum_n y_{Rn}(x)y_{Rn}^{*}(x)S_{nrn}(\omega) \tag{48a}$$

$$S_{zz}(x,\omega)=\sum_n z_{Rn}(x)z_{Rn}^{*}(x)S_{nrn}(\omega) \tag{48b}$$

$$S_{\alpha\alpha}(x,\omega)=\sum_n B^{-2}\alpha_{Rn}(x)\alpha_{Rn}^{*}(x)S_{nrn}(\omega) \tag{48c}$$

It can be seen that such a reduction of PSD matrices to diagonal forms will greatly reduce the computational effort in a quadratic order. The next question is how the

cross-terms affects the results. A parameter study for this effect is presented later.

Like the previous paper[7], following assumptions in the formulation remain: (a) Quasi-static assumption is for buffeting force so that the aerodynamic admittance functions is unit; (b) Strip assumption[1] holds for the spatial correlation of the buffeting force along the deck; and (c) Changes of the mean angle of attack along the deck and the large static displacement due to mean wind speed are neglected.

5. Coupled buffeting of the Akashi Kaikyo Bridge model

5.1 *Turbulence characteristics*

(a) *Fitted wind-tunnel turbulence properties* by direct statistic analysis of turbulence record: The time-history records of turbulence generated in wind tunnel for the full-model test of the Akashi Kaikyo Bridge are directly analyzed, and then generalized into analytical close-forms of statistical properties. The scaled (from model to prototype scale) spectra and point cospectrum of the turbulence can be expressed as,

$$\frac{fS_u(f)}{\overline{u^2}} = \frac{5.11f_r}{(1+7.05f_r)^{5/3}}, \qquad \frac{fS_w(f)}{\overline{u^2}} = \frac{6.15f_r}{1+3.7f_r^{5/3}}$$
$$\frac{fCo_{uw}(f)}{\overline{u^2}} = \frac{-1.5f_r}{(1+2.94f_r)^{2.4}} \tag{49}$$

where $\overline{u^2}$ is mean square of horizontal gust component (u). Compared to the set in the previous paper[7], this set is more general by using the normalized frequency f_r = fz/U, where z is the height. The coherence functions can be expressed in our proposed forms as follows,

$$Coh_{u_Au_B}(f) = C_0^u(dx)\exp(-f\,C_x^u dx/U) \tag{50}$$
$$Coh_{w_Aw_B}(f) = C_0^w(dx)\exp(-f\,C_x^w dx/U) \tag{51}$$
$$Coh_{u_Aw_B}(f) = 0.5\left[Coh_{u_Au_B}(f) + Coh_{w_Aw_B}(f)\right] \tag{52}$$

where $C_x^u = 12$, $C_x^w = 8$;

$$C_0^u(dx) = (1 - 0.001dx - 0.0003dx^2)$$
$$C_0^w(dx) = (1 - 0.03dx + 0.0002dx^2) \tag{53}$$

(b) *Reported target turbulence properties*: following turbulence properties have been reported as the targets of the wind-tunnel turbulence simulation of the full model test (see Katsuchi[4] 1997). Hino spectrum holds for S_u as follow,

$$\frac{f.S_u(f)}{\overline{u^2}} = 0.4751\frac{f/\beta}{\left\{1+(f/\beta)^2\right\}^{5/6}} \tag{54}$$

where, $$\beta = 0.01718\frac{\alpha K_r U_{10}}{I_u^3}\left(\frac{z}{10}\right)^{(2m-3)\alpha-1}$$

α = 1/8; K_r = 0.0025; I_u is turbulence intensity, m=3 is an empirical factor, U_{10} is mean wind speed at the height of 10m. The auto-spectrum S_w is following the Busch and Panofski form as follow,

$$\frac{f.S_w(f)}{\overline{w^2}} = 0.6320\frac{f_r/f_{max}}{1+1.5(f_r/f_{max})^{5/3}} \tag{55}$$

where f_r = f z/U_z, f_{max}=0.4 is an empirical factor. The Von Karman spatial coherence has been reported to agree very well with the measured coherence. However, its analytical forms are so complicated for engineering use. A modified form for these coherence functions have been employed by Katsuchi[4] (1997) as follows,

$$Coh_{ab}(f,dx) = \exp\left\{-\frac{cB_1}{\pi}\frac{dx}{L}\sqrt{1+(2\pi/B_1)^2(fL/U)^2}\right\} \tag{56}$$

in which $L=L_u^x$=70cm for Coh_{uAuB}; $L=L_w^x$=40cm for Coh_{wAwB}; B_1=0.747; and decay factor c=8. Note that all the coherence function here is defined in its square form.

5.2 *Aeroelastic coupling in the response*

The buffeting of the Akashi Kaikyo bridge model is analyzed by the present method with the fitted turbulence properties at eight wind speeds: 30, 36, 44, 54, 63, 71, 76 and 80m/s. Other data are similar to those of previous paper[7]: turbulence intensity I_u=9.6%, I_w=6%; the flutter derivatives and static coefficients for the modified cross-section at zero angle of attack are used; modal structural logarithmic decrements are 0.03; number of modes is 32; frequency step is 0.001Hz; time step is 0.1s.

Thanks to refined data and programming techniques, the agreements between calculated and experimental results, which have been reported in the previous paper[7], can be seen better via Fig.6b for the frequency domain and Fig.7 for the time domain analysis. A comparison of response spectra at 76m/s is shown in Fig.3. Very good similarity between those from time and frequency domain analysis with the measured ones[11] are obtained. Similar results are also obtained at other wind speeds[8].

Fig.2 extensively shows the evolution of the motion-coupled modes #9 and #10 from their mechanical modes at U=0 to higher wind speeds. The most interesting feature in these evolutions is the appearance and development of the vertical component in the modes, mainly on the right eigenvector, which makes the vertical response spectrum evolves spectacularly with wind speeds as seen in Fig.5. Such evolution makes the response become strongly 3-motion coupling, represented by PSD's peaks for all response components at the same modal frequency, especially at #10, as observed in Fig.3. It is interesting to note that although evolving to a smaller extent than the mode #10 at low wind speeds, mode #9, the 1st torsional mode, is quickly enhanced at high wind speeds and develops to flutter instability. These developments are indicated by the evolution of aerodynamic damping, as shown in Fig.4.

In modes #9 and #10 (Fig.2), the development of vertical components are only in the right eigenvectors, whereas the left still basically keeps almost unchanging, except the appearances of imaginary components. In the meaning of the right eigenvector, representing the mode shape, and the left eigenvector, representing the modal force, it can be interpreted that in these modes, all the 3 motions of the bridge deck are excited by only drag force and moment. A closer look reveals that the vertical motion is mainly excited by the moment. This relation is dictated by the unsteady coefficient L_α, which is the coefficient for 'aeroelastic lift induced by rotational

response'. The vertical component appears in the mode shapes therefore can be interpreted as the aeroelastic effects, mainly governed by the unsteady coefficient L_α.

5.3 *Cross-terms effects*

As mentioned, the only difference of the MDOF from the SDOF spectral formulation is the cross-terms of the modal buffeting force PSD matrix S_{QbQb}. The MDOF spectral analysis is quite sophisticated and very time-consuming, while the SDOF spectral analysis is much simpler and requires very small computational efforts.

A comparative checks of the effects of the cross-terms is made and presented in Figs.6a and b. Fig.6a shows the effects on the response spectra at relatively high wind speed of 76m/s. Notable, however small, differences between results of the two MDOF or SDOF spectral analyses can be seen especially for closely-spaced modes. The vertical spectrum is therefore the most affected by this effect. Less effect can be seen for torsional spectrum, whereas almost no effect is obtained for the horizontal spectrum. More comparisons at other wind speeds can be found in Minh[8] (1998) indicating that the extent of the differences is more pronounced at higher wind speeds. A general look at the effects can be achieved by Fig.6b, which shows the effects on the RMS and the average maximum amplitude (AMA) at a wide range of wind speeds. Very small differences are obtained for all response components. The vertical response, however, shows notably larger differences at higher wind speeds. The maximum errors obtained at 80m/s are 7.8%, 0.7% and 1.2% for vertical, horizontal and torsional response respectively.

Therefore, it can be concluded that for the analysis in frequency domain, the SDOF spectral formulation, which is more conventionally used, is still effective enough for this case. Use of SDOF spectral formulation will significantly reduces the computational efforts and many complications in formulation and programming.

5.4 *A parameter study on turbulence inputs*

The effects on the response by the differences between the fitted properties of the wind-tunnel turbulence in the full model test and the natural turbulence properties from literature have been pointed out in the previous paper[7]. It has been pointed out that the use of Davenport's coherence function greatly overestimates the horizontal response observed in the full model test.

In this paper, a parameter study is made for the reported target turbulence properties. Fig. 7 shows the comparison of results between the default case (a) 'fitted wind-tunnel turbulence properties' and case (b) 'reported target turbulence properties' as presented in Sec.5.1. The vertical and the torsional response from both cases well agree to each other. The horizontal response of case (b), however, is still around 2 times higher than that of case (a). This result was also reported by other works using this set of turbulence input (Katsuchi[4]).

The main reason can be seen in Fig.8a, which shows the comparison between spatial coherence from both cases. It can be noted that the modified Von-Karman coherence, although a little bit smaller than the wind-tunnel coherence for small distances, still higher than the wind-tunnel coherence for a far distance, such as dx=50m. Fig.8b gives a clearer representation for this note. This figure shows the comparison of coherence values versus separate distance at the frequency f=0.039, which obviously influences directly on the horizontal response since this response is dominated by mode #1 of around f=0.039Hz. It can be seen clearly that the modified Von-Karman coherence overestimates the wind-tunnel coherence for a far distance, and this overestimation continues very far following the exponential form. On the contrary, the wind-tunnel coherence appears to decrease and vanish very quickly, say, after 56 m for u component. For a very long span bridge, the coherence for very far distance, however small, still plays an important role to affect the response of the first mode. That is the reason why the modified Von Karman, though better fitted to the wind-tunnel turbulence, still makes the calculated horizontal response higher than experimental one.

These interesting results prove the effectiveness of the idea of using the fitted wind-tunnel turbulence properties by direct analysis of turbulence records as input for a good match with the condition in the wind tunnel, rather than accepting the ready-made turbulent properties for calculation.

6. Comparison with Conventional Method

The conventional method in frequency domain, which is sometimes called 'Admittance method' or 'Admittance Single-mode method', was developed by Davenport[1] (1962), making use of the well-developed theory of spectral analysis for random vibration. The method is applied one-by-one for each chosen *mechanical mode*, and then the response spectra of many modes are summed to get the total response spectrum. There is neither concept of aeroelastic effects nor coupled response. The modal logarithmic decrements due to the modal aerodynamic damping are determined by very simple formula based on quasi-static theory as follows,

$$\delta_r^v = \frac{1}{4}\frac{\rho U C_L' B}{n_r \overline{m}} \qquad \delta_r^h = \frac{1}{2}\frac{\rho U C_D B}{n_r \overline{m}} \qquad \delta_r^t = \frac{1}{4}\frac{\rho U C_M' B^2}{n_r \overline{m} k} \tag{57}$$

where $\delta_r^v, \delta_r^h, \delta_r^t$ are logarithmic decrements for vertical, horizontal and torsional modes respectively, n_r: frequency of r^{th} mode, $\overline{m}$: mass per unit length, k: radius of gyration. It can be seen that these aerodynamic dampings are linear with wind speed. More details of the method can be found in Davenport[1] (1962).

A comparison of this conventional Admittance Single-Mode (ASM) method and the presented Aeroelastic Complex Mode (ACM) method in frequency domain is made. The differences of the ASM method from ACM method can be resumed as follows,

+ Using the set of mechanical modes
+ Following SDOF spectral formulation for analysis, similar to the formulation in Sec.4.2
+ Formulating the aerodynamic dampings by the quasi-static assumption as Eqs.(57)

The buffeting responses at the mid-span of the main span of the Akashi-Kaikyo Bridge model are calculated by both methods under the same condition of the fitted wind-tunnel turbulence inputs (Sec.5.1a). As experienced from a parameter study in the previous paper[7], there are

five significant modes for the response at the mid-span of the bridge, which yield reasonable results for ACM method. Their mechanical descriptions are as follows. Mode #1 is the 1st horizontal mode; Mode #2 is the 1st vertical mode; Mode #8 is the 3rd vertical mode; Mode #9 is a coupling mode between the 1st torsional and the 3rd horizontal; Mode #10 is also a coupling mode between the 1st torsional and the 3rd horizontal but in opposite sign. Then, for both ASM and ACM methods, these modes are selected for calculation in this section.

Fig. 9 presents the comparison of response spectra from the two methods at the wind speed of 63m/s. A common difference is that all the peaks from ACM are at smaller frequencies than those from ASM are. Therefore, due to higher values of turbulent spectra at smaller frequency, the amplitudes of ACM's peaks are higher than those of ASM's peaks are. In the vertical spectrum, the ASM result does not have peaks at frequency of modes #9 and #10 as well as their evolutions with wind speed like those in ACM results. This is because these vertical responses at mode #9 and #10 are due to aeroelastic effects, which can not be captured by the ASM method. For horizontal response, since mode #1, which is actually not so much affected by aeroelastic phenomena, exclusively dominates the response, very good agreement between the two methods is observed. For torsional response, the ASM method very much underestimates the response due to its overestimation of the torsional aerodynamic damping. It is noted that compared with aerodynamic damping computed by complex mode method (Fig.4), the aerodynamic damping estimated by Eq.(57) gives very fair results for vertical and horizontal motions, while yields very much over-estimated results for torsional motions[8].

Fig.10 shows the comparison of the RMS of the responses from the two methods at eight wind speeds. The comparison reflects very well the observations in Fig.9. The ASM method underestimates the vertical response because it can not capture the vertical response at mode #9 and #10. As wind speed increases, the aeroelastic phenomena is more pronounced, making the vertical response by ACM method increase quickly due to the development of aeroelastic couplings at mode #9 and #10, as seen in Fig.5. The discrepancies between the two methods thus increase as well.

Nevertheless, the ASM method, attracted by its simplicity, could be used at the preliminary stage of design. The expected errors are that it would underestimate vertical response especially at high wind speeds; very much underestimate torsional response; and give fair result for horizontal response. Assumption of zero torsional aerodynamic damping is recommended for conservative results as also seen in Fig.9.

7. Concluding Remarks

The buffeting analysis by complex modes, which is called Aeroelastic Complex Mode method has been extensively presented with detailed formulation. The versatility of the method, which is capable to solve the coupled buffeting in both time and frequency domains with clear representation of the dynamic behaviors of long span bridges in term of aeroelastic complex modes, could benefit much for further sophisticate problems for bridges such as vibration control, etc.

A further parameter study on turbulence inputs, mainly on the effect of the use of the modified Von Karman coherence, has revealed its potential of overestimating the full model's horizontal response. The parameter study has also proved the effectiveness of the fitted wind-tunnel turbulence properties, especially the fitted coherence function for the buffeting of full model of the Akashi Kaikyo Bridge. A detailed look into the frequency domain spectral formulation was provided, from which the conventional and simple SDOF spectral formulation could be proved still effective enough. Lastly, a comparison with the conventional buffeting method not only confirmed the effectiveness of the new method, but also gave suggestions of how to use the conventional method for the early stage of bridge design.

As the results, a better understanding on the coupled buffeting of long-span bridges is achieved, which effectively explains the observed dynamic behaviors of the full model of the Akashi Kaikyo Bridge in wind tunnel. These investigations, including those in the previous paper[7], prove the effectiveness and accuracy of the new method, which is suggested to be used for buffeting analysis of long-span bridges in future.

References

1. Davenport, A.G. (1962), "Buffeting of a Suspension Bridge by Storm Winds", *J. of Struct. Division.*, ASCE, Vol.88, No.ST3, pp. 233-268.
2. Dung, N.N., Miyata, T. and Yamada, H.(1996). "The Mode Tracing Method for Flutter of Long Span Bridges", *Proc., 14th Nat. Symp. on Wind Eng.*, Japan.
3. Dung, N.N., et al. (1997), "Flutter Responses in Long Span Bridges with Wind Induced Displacement by the Mode Tracing Method", *Proc., 8th Nat. US Conf. of Wind Eng.*, Baltimore, USA, 1997.
4. Katsuchi, H. (1997), *An Analytical Study on Flutter and Buffeting of the Akashi-Kaikyo Bridge*, Master Thesis, The Johns Hopkins University, USA.
5. Jain, A., Jones, N. P., and Scanlan, R. H. (1996), "Coupled Flutter and Buffeting Analysis of Long-Span Bridges," *J. Struct. Eng.*, ASCE, 122(7).
6. Minh, N. N., Miyata, T., and Yamada, H. (1997), "Numerical Simulation of Wind Turbulence and Buffeting Analysis of Long Span Bridges," *Proc., 4th Asia-Pacific Symp. on Wind Eng.*, Australia
7. Minh, N.N., Miyata, T. and Yamada, H. (1998), "Complex-mode Buffeting Analysis of Long-Span Bridges", *J. of Struct. Eng.*, JSCE, Vol.44A
8. Minh, N.N. (1998), *Aeroelastic Complex-mode Method for Coupled Buffeting of Long-span Bridges*, Dissertation, Dept. of Civil Engineering, Yokohama National University, Japan.
9. Miyata, T. and Yamada, H. (1988), "Coupled Flutter Estimate of a Suspension Bridge", *J. of Wind Eng.*, Vol. 37, Japan.
10. Miyata, T., Yamada, H. and Kazama, K. (1995), "On Application of the Direct Flutter FEM Analysis for Long Span Bridges," *Proc., 9th Int. Conf. on Wind Eng.*, New Delhi, India
11. The Honshu-Shikoku Bridge Authority (HSBA) (1992), *Report on Full Model Test of the Akashi Kaikyo Bridge*, (in Japanese)

(Received on September 18, 1998)

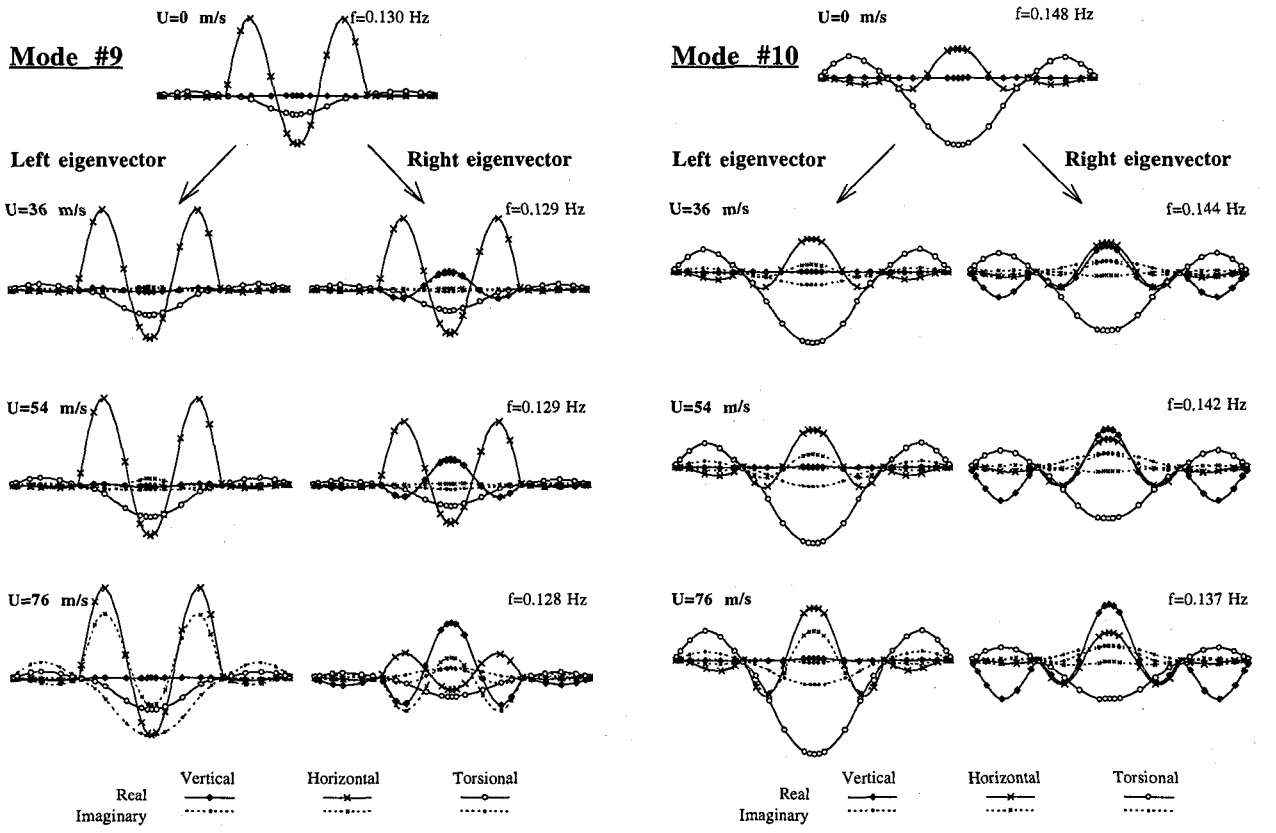

Figure 2 Evolution of the aeroelastic complex modes #9 & #10 with wind speeds

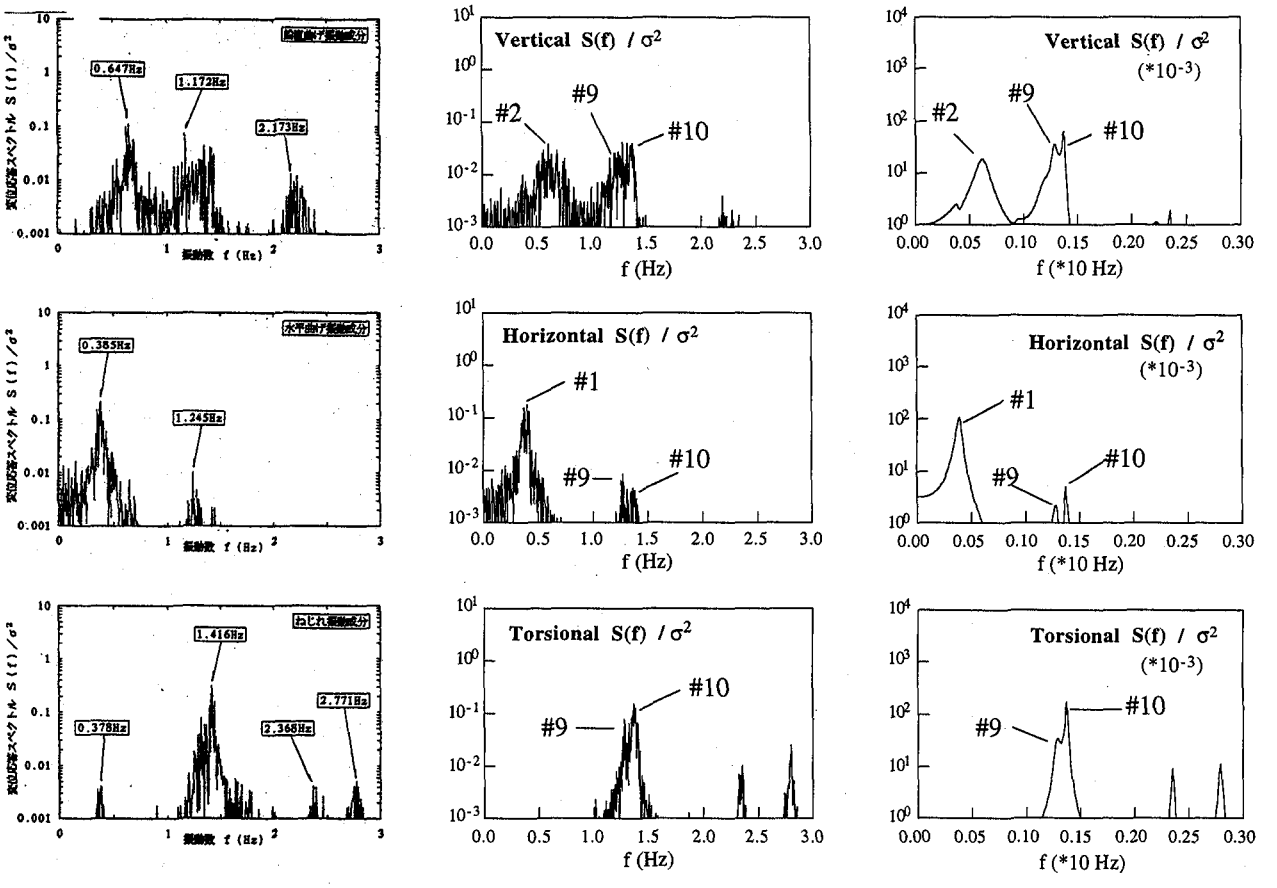

Measured spectra[11] By Time-domain analysis By Frequency-domain analysis

Figure 3 A comparison between experimental and calculated response spectra at U=76m/s (units in model scale)

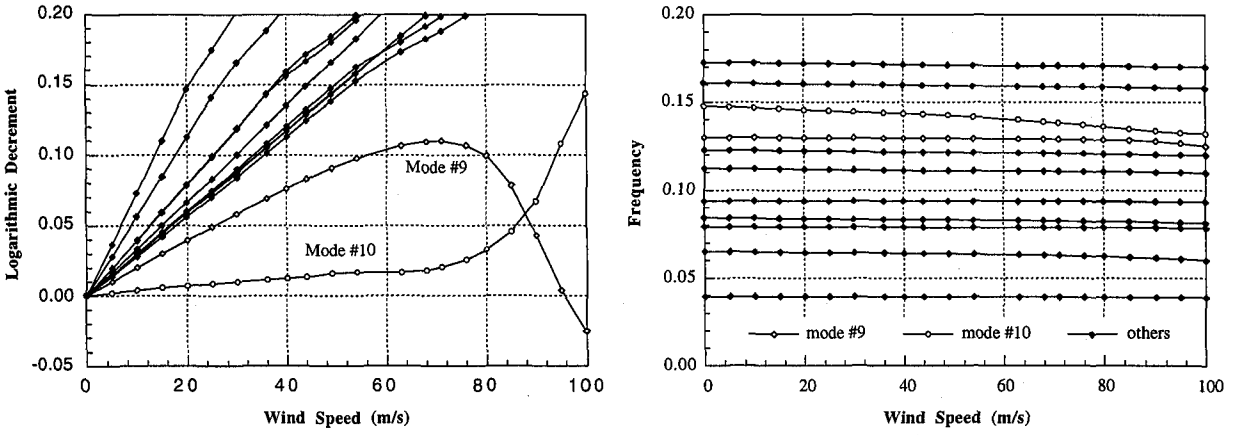

Figure 4 Tracing the modal aerodynamic damping and frequency with wind speeds by the Mode tracing method

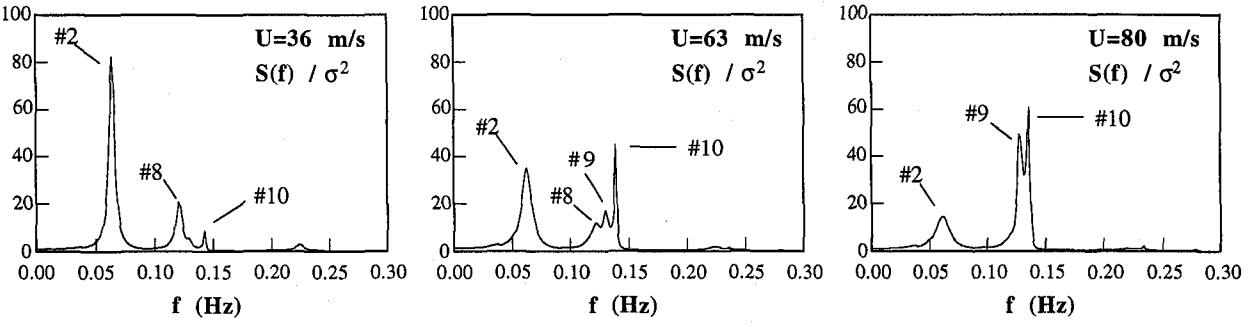

Figure 5 Evolution of vertical response spectrum with wind speed (units in prototype scale)

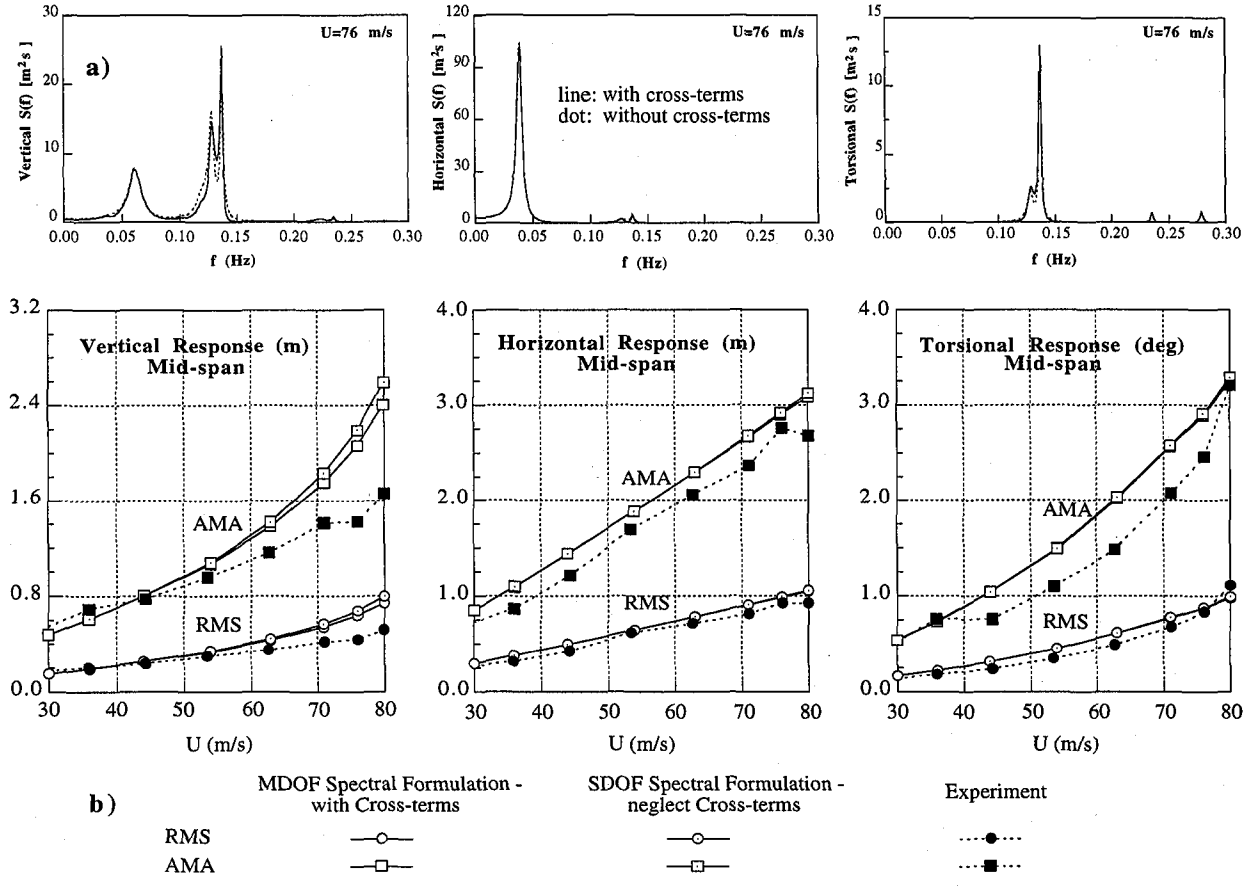

Figure 6 Effects of the cross-terms of modal buffeting force PSD matrix on **a)** Response spectra and **b)** RMS/AMA (resulted from Aeroelastic Complex Mode (ACM) method in frequency domain)

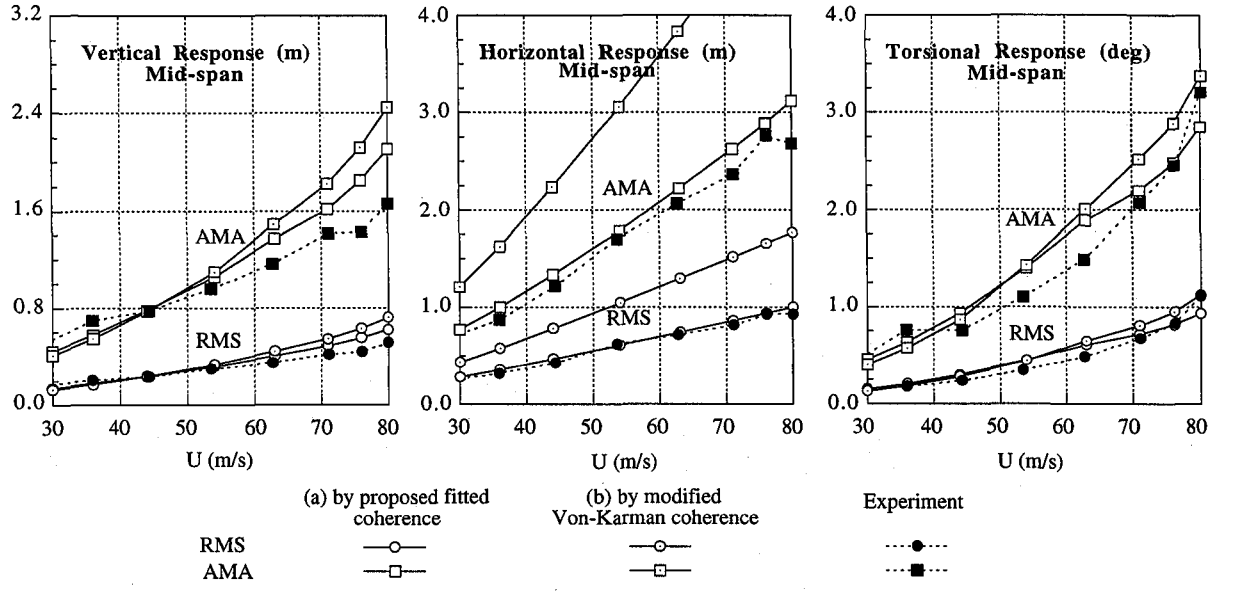

Figure 7 Effects of different turbulence inputs on RMS & AMA (by ACM method in time domain)

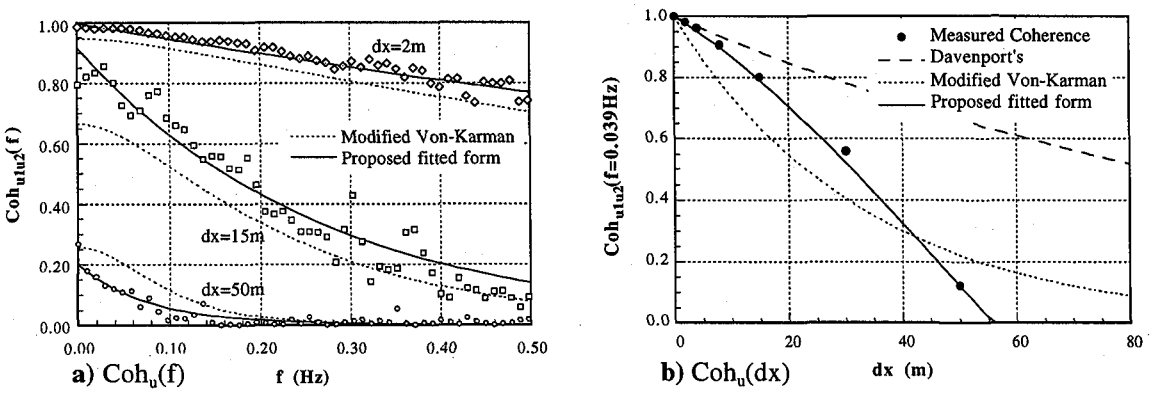

Figure 8 Comparison of coherence function of u-turbulent velocity

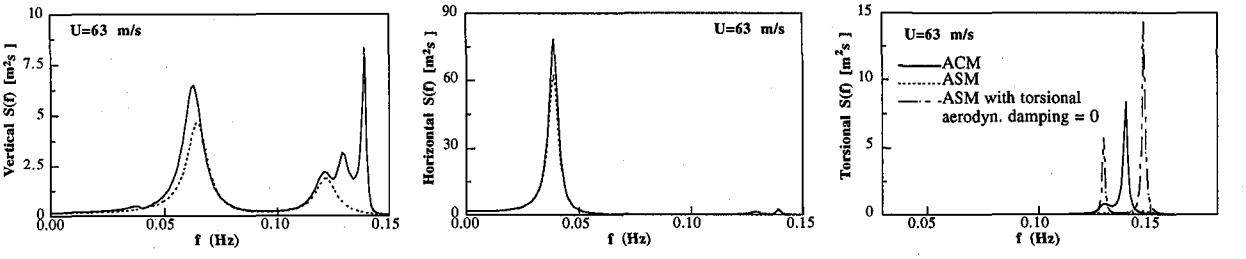

Figure 9 A spectra comparison between ACM and ASM methods at U=63 m/s

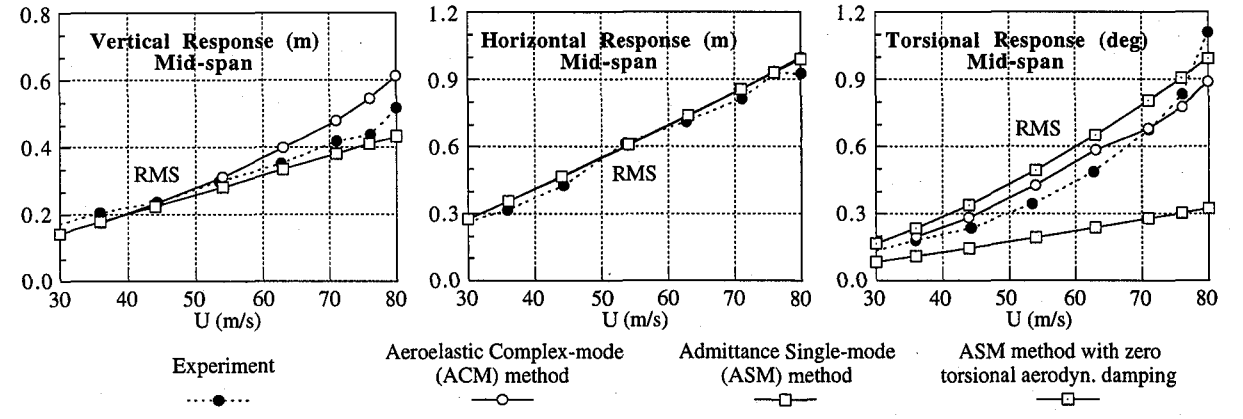

Figure 10 Responses' RMS comparison between ACM and ASM methods

Appendix A: With the self excited force by Eq. (2), the corresponding force vector at each of shear nodes A or B in the local coordinate xyz (Fig.11) is

$$\begin{Bmatrix} f_x \\ f_y \\ f_z \\ m_x/B \\ m_y/B \\ m_z/B \end{Bmatrix} = \begin{Bmatrix} \cdots \\ L_{ae} \\ D_{ae} \\ M_{ae}/B \\ \cdots \\ \cdots \end{Bmatrix} = -\rho\pi l_e B^2 \mathbf{F}_w^L \begin{Bmatrix} \ddot{u}_x \\ \ddot{u}_y \\ \ddot{u}_z \\ \ddot{\phi}_x B \\ \ddot{\phi}_y B \\ \ddot{\phi}_z B \end{Bmatrix} \qquad \text{(A1)}$$

where

$$\mathbf{F}_w^L = \begin{bmatrix} 0 & 0 & 0 & 0 & 0 & 0 \\ 0 & L_{yR}+iL_{yI} & L_{zR}+iL_{zI} & L_{\alpha R}+iL_{\alpha I} & 0 & 0 \\ 0 & D_{yR}+iD_{yI} & D_{zR}+iD_{zI} & D_{\alpha R}+iD_{\alpha I} & 0 & 0 \\ 0 & M_{yR}+iM_{yI} & M_{zR}+iM_{zI} & M_{\alpha R}+iM_{\alpha I} & 0 & 0 \\ 0 & 0 & 0 & 0 & 0 & 0 \\ 0 & 0 & 0 & 0 & 0 & 0 \end{bmatrix} \qquad \text{(A2)}$$

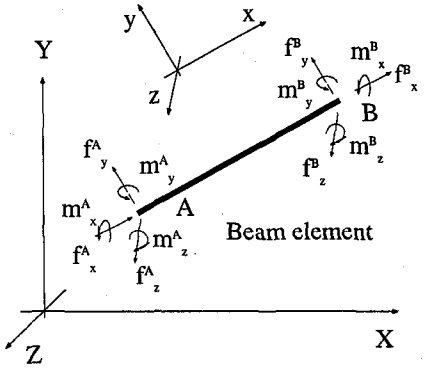

Figure 11 Beam element

where l_e is the element length. The right hand side vector is the nodal accelerations corresponding to the nodal forces in the left hand side, which are depicted on Fig.11.

Appendix B: Procedure of the Mode Tracing method

INITIAL CALCULATION

1. Form mass matrix **M**, stiffness matrix **K** of the bridge structure by FEM
2. Perform eigen-analysis for the bridge structure (at U=0) by

$$\det|\mathbf{K}-\lambda_0^2\mathbf{M}|=0$$

to obtain the set of mechanical modal properties, including eigenvalue λ_0^2 and mode shape v_0, which serve as initial value of the iteration.

FOR EACH MODE

A. Initialize

a. *Initialize* corresponding λ_0^2 and v_0, which mean the eigen-properties at U=0

b. *Choose wind speed step* ΔU. The iteration is started from $U = \Delta U$

B. For each wind speed step

(Outer loop - step index: ...,U-ΔU,U,...)

a. *Initialize*

1. Approximate eigenvalue and mode shape

$$\lambda_{U,0}^2 = \lambda_{U-\Delta U}^2; \quad \mathbf{v}_{U,0} = \mathbf{v}_{U-\Delta U}$$

2. Trial value of the modal frequency

$$\omega_{U,0} = \omega_{U-\Delta U} = \sqrt{\lambda_R^2+\lambda_I^2} \quad \text{where } \lambda_R+i\lambda_I = \sqrt{\lambda_{U-\Delta U}^2}$$

b. *For each trial value of modal frequency*

(Inner loop - step index: i=1,...)

1. Calculate the trial value of K_i

$$K_{U,i} = \omega_{U,i-1}B/U$$

2. Evaluate the unsteady coefficients at $K_{U,i}$

3. Flutter Equation (7a) is formed for the target mode at wind speed U

$$\det|\mathbf{K}-\lambda_{U,i}^2\mathbf{M}_F(K_{U,i})|=0$$

4.Solve the eigen-problem by the power method with inverse iteration and shifting eigenvalue technique to obtain $\lambda_{U,i}^2$ and $\mathbf{v}_{U,i}$

$$\left[\frac{1}{(\lambda_{U,i}^2-\lambda_{U,i-1}^2)}\left(\mathbf{K}-\lambda_{U,i-1}^2\mathbf{M}_F\right)-\mathbf{M}_F\right]\mathbf{v}_{U,i}=\mathbf{0}$$

where previous value $\lambda_{U,i-1}^2$ is a shift to make the target mode dominant

5. Confirm the similarity between the newly-calculated mode shape $\mathbf{v}_{U,i}$ with the previous $\mathbf{v}_{U,i-1}$ to keep accurate tracing direction

6. Compare the newly-calculated eigenvalue $\lambda_{U,i}^2$ with the previous $\lambda_{U,i-1}^2$

+ if the error is not acceptable, re-initialize the new $\omega_{U,i}$ by

$$\omega_{U,i} = \sqrt{\lambda_R^2+\lambda_I^2} \quad \text{where} \quad \lambda_R+i\lambda_I = \sqrt{\lambda_{U,i}^2}$$

or by extrapolation with the secant line technique from previous solutions for faster convergence. The iteration then return to step 1 for the next step of i

+ If the error is negligibly small, take the solution at wind speed U,

$$\lambda_U^2 = \lambda_{U,i}^2; \qquad \mathbf{v}_U = \mathbf{v}_{U,i}$$

and calculate corresponding aerodynamic damping,

$$\delta_U = 2\pi\frac{\lambda_I}{\sqrt{\lambda_R^2+\lambda_I^2}} \quad \text{where } \lambda_R+i\lambda_I = \sqrt{\lambda_U^2}$$

then go to the next step of wind speed. If wind speed reaches a specified maximum value, stop tracing the mode.

General rule of notations:

$$A_{w,i}$$

where,

- Subscript 'w' stands for the outer loop of wind speed
  . Current windspeed: w = U
  . Previous wind speed: w = U-ΔU
- Subscript 'i' stands for the inner loop, i=1,...